Static and dynamic properties of polymer brush with topological ring structures: Molecular dynamic simulation*

Wu-Bing Wan(万吴兵)[1,2], Hong-Hong Lv(吕红红)[1,2], Holger Merlitz(候格)[1], and Chen-Xu Wu(吴晨旭)[1,2,†]

[1] *Institute of Softmatter and Biometrics, Xiamen University, Xiamen* 361005, *China*

[2] *Collaborative Innovation Center of Chemistry for Energy Materials, Xiamen University, Xiamen* 361005, *China*

(Received 14 March 2016; revised manuscript received 17 June 2016; published online 25 August 2016)

By defining a topological constraint value (rn), the static and dynamic properties of a polymer brush composed of moderate or short chains with different topological ring structures are studied using molecular dynamics simulation, and a comparison with those of linear polymer brush is also made. For the center-of-mass height of the ring polymer brush scaled by chain length $h \sim N^{\nu}$, there is no significant difference of exponent from that of a linear brush in the small topological constraint regime. However, as the topological constraint becomes stronger, one obtains a smaller exponent. It is found that there exists a master scaling power law of the total stretching energy scaled by chain length N for moderate chain length regime, $F_{\rm ene} \sim N\rho^{\nu}$, for ring polymer brushes, but with a larger exponent ν than 5/6, indicating an influence of topological constraint to the dynamic properties of the system. A topological invariant of free energy scaled by $\langle c\rangle^{5/4}$ is found.

Keywords: ring polymer, topological invariant, scaling

PACS: 61.41.+e **DOI:** 10.1088/1674-1056/25/10/106101

1. Introduction

Polymer brushes are depicted as layers of long-chain polymer molecules tethered by one end to a substrate surface. The study of polymer brush is important in many applications, such as polymer adhesion, colloidal stabilization, lubrication, and DNA segregation in bacteria.[1–4] In recent years, there has been a great deal of interest in the properties of ring polymer for mathematical,[5–10] simulational,[11–13] and experimental[14–18] scientists. The configuration of ring polymer in melt or solution plays a significant role in most biological systems,[19,20] making it a hot research topic in polymer physics. Flory theory suggested that behaviors of linear polymer chains are similar to those of trivial Gaussian chains, for gyration radius, both complying with a Flory exponent $\nu = 1/2$ scaled as $R_{\rm G} \sim N^{\nu}$ in melts due to the volume-excluded effect. However, even such a simple scaling law is not suitable for ring polymers, which have been confirmed by simulations[21–25] and experiments.[26] Based on mean-field theory, Cates and Deutsch pointed out that unconcatenated ring polymers have a scaling exponent $\nu = 2/5$, an intermediate value between collapsed $(1/3)$ and Gaussian $(1/2)$ types,[9] a conclusion supported by simulations.[21–24] Several new observations found that a sufficiently long ring chain has a size scaling $N^{1/3}$ close to that of a collapsed chain.[25] For ring polymers in good solvent and under high grafting density, He[27] found that, for the scaling law $R_{\rm G} \sim N^{\nu}$, the exponent ν of ring polymer chain is smaller than the linear's. He also found that the thickness of ring polymer brush has a power scaling law $h \sim N\rho^{0.27}$ rather than $h \sim N\rho^{1/3}$ for a linear polymer brush composed of moderate chain length.

In 2011, combining the topological volume fraction and a classical van der Waals theory of fluids, Sakaue constructed a mean-field theory by taking into account the many-body effect of the topological origin in dense systems.[28] Suzuki studied the topological constraint in ring polymer under θ conditions, and demonstrated that the Flory exponent ν for ring polymer with topological constraint is larger than $1/2$ at the θ-temperature of a linear polymer.[29] Trefz performed large scale molecular dynamics simulation to study the scaling behaviors of unknotted ring polymer and knotted ring polymer in a melt, and found that the size scaling for a typical ring of small N depends on its knot type.[30]

Ring polymers differ from their linear counterparts by the topological constraints which force a ring polymer conformation to stay within the topological state of preparation.[31] However, it has not been established how to correlate analytically the topological feature of polymeric molecules with ring polymer brush structure. In this work we quantitatively analyze the influence of topological constraint on ring polymer brushes. Using MD simulation, we investigate the static and dynamic scaling properties of ring polymer brushes in a good solvent. In Section 2, the polymer simulation model and the topological constraint we used are described. In Section 3, the structure of ring polymers with different topological features

*Project supported by the National Natural Science Foundation of China (Grant Nos. 11374243 and 11574256).

†Corresponding author. E-mail: cxwu@xmu.edu.cn

© 2016 Chinese Physical Society and IOP Publishing Ltd

and their scaling behaviors are presented, followed by a discussion of their dynamic properties. We also investigate the behaviors of end-monomers for a polymer chain and carry out an isothermal compression of the brush in order to study its stretching energy. Our conclusion is summarized in Section 4.

2. Simulation model

In our simulation, the coarse-grained bead-spring model was used to study ring polymer brushes. Each chain consists of a sequence of identical small rings composed of a certain number of connected monomers. The number of rings within a chain and the number of monomers within each small ring define the basic topological feature for a ring polymer chain. The brush was modeled as a collection of freely jointed bead spring polymer ring chains, with one end attached to a planar surface, forming a 10×10 square grid. We chose a simulation box $L \times L \times L_z$ with a periodic boundary condition in x and y directions. We used the open source molecular dynamics package LAMMPS[32] and Lennard-Jones (LJ) system of units to perform molecular dynamic simulations. The total interaction potential of connected monomers is given by

$$U_{\rm tot} = U_{\rm FENE} + U_{\rm LJ} + U_{\rm WALL}, \tag{1}$$

where $U_{\rm FENE}$, $U_{\rm LJ}$, and $U_{\rm WALL}$ are FENE potential, LJ potential, and 9-3 type LJ-wall potential respectively. All beads interact among themselves via a shifted LJ potential with a cutoff at its minimum, so as to model the repulsive short-range potential in good solvent condition.

$$U_{\rm LJ}(r) = 4\varepsilon \left[\left(\frac{d}{r}\right)^{12} - \left(\frac{d}{r}\right)^{6} - \left(\frac{d}{r_{\rm c}}\right)^{12} + \left(\frac{d}{r_{\rm c}}\right)^{6} \right], \tag{2}$$

where d is the bead diameter, ε is the depth of the potential, r is the distance between the particle, and $r_{\rm c}$ is the cutoff distance. It is widely known that, solvent quality influences the conformations of polymer brushes, leading to different behaviors under different solvent conditions. In a good solvent, a repulsive interaction between polymer monomers and solvent molecules is favorable, and the entropy loss due to overlapping of chains will cause polymer chains to expand. Neighboring monomers along the polymer chains interact with each other through a finitely extensible nonlinear elastic (FENE) bond potential

$$\begin{aligned} U_{\rm FENE} = & -0.5KR_0^2 \ln\left[1 - \left(\frac{r}{R_0}\right)^2\right] \\ & + 4\varepsilon\left[\left(\frac{\sigma}{r}\right)^{12} - \left(\frac{\sigma}{r}\right)^{6}\right] + \varepsilon, \end{aligned} \tag{3}$$

where the first attractive term extends to $R_0 = 1.5\sigma$, the maximum extent of the bond, and the 2nd repulsive term is cutoff at $2^{1/6}\sigma$, the minimum of the LJ potential. The spring constant K is specified as $30\varepsilon/\sigma^2$, and r is the lengths of the bond. In our simulation, we set an average bond length of $l_v = 0.97\sigma$. The first monomer (grafted monomer) was grafted at a substrate located at $z = 0$ and modelled by a 9–3 type LJ-wall potential(9 and 3 corresponding the index of the formula)

$$U_{\rm WALL} = \varepsilon \left[\frac{2}{15}\left(\frac{d}{r}\right)^{9} - \left(\frac{d}{r}\right)^{3} \right]. \tag{4}$$

This 9–3 type interaction can be obtained by an integration over a $3d$ half-lattice of standard Lennard-Jones 12–6 particles. In our calculation, only its short-range repulsion is applied. To compare with linear polymer brushes with chain length N and grafting density σ_g, ring polymer brushes with chain length $N_R = 2N$ and grafting density $\sigma/2$ were studied so that the total number of monomers was strictly kept identical in both cases. The linear chain lengths $N = 31, 61$ corresponding to ring chain lengths $N = 62, 122$ were studied. Here it should be noted that corresponding to a fixed chain length, we studied ring polymers containing different numbers of rings. For example, for chain length 62, brushes consisting of ring polymers with ring numbers $rn = 1, 2, 3, 4, 5, 6, 10$ were investigated. Here ring number is treated as a topological variable. We set a monomer which connects the mid-monomer of the top ring of the ring polymer as the end-monomer. The motion of any effective monomers (nongrafted monomer) was governed by the Langevin equation

$$m\frac{{\rm d}^2\boldsymbol{r}_i}{{\rm d}t^2} + \varsigma\frac{{\rm d}\boldsymbol{r}_i}{{\rm d}t} = -\frac{\partial U_{\rm TOT}}{\partial \boldsymbol{r}_i} + \boldsymbol{F}_i, \tag{5}$$

where $m = 1$ is the monomer mass, r_i is the position of the i-th monomer, and ς is the friction coefficient. F_i is a random Gaussian force satisfying the correlation function

$$\left\langle \boldsymbol{F}_i(t) \cdot \boldsymbol{F}_j(t') \right\rangle = 2k_{\rm B}T\varsigma\delta_{ij}\delta_{\alpha\beta}.$$

In our simulation, the diameter of monomers is $d = 1.0$, and $k_{\rm B}T = 1.2\varepsilon$, where $k_{\rm B}$ is the Boltzmann constant and T is the absolute temperature. For our simulation, each time step is set to be $\Delta t = 0.0015\tau_{\rm LJ}$, where

$$\tau_{\rm LJ} = (md^2/\varepsilon)^{1/2}$$

is the oscillation time of a monomer inside the LJ potential, and a friction coefficient $\varsigma = {\tau_{\rm LJ}}^{-1}$ was implemented. The friction leads to an over damped motion on length scales of bead size and hence to a Brownian motion under the approximation of an immobile solvent. The initial brush conformation was set up as an array of stretched chains before they relax by implementing 6×10^7 simulation steps. Figure 1 displays ring polymers with different topological constraints.

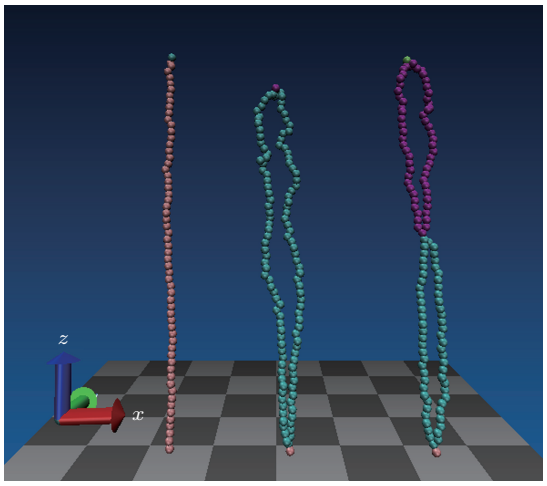


Fig. 1. (color online) Ring polymer brush conformation with different topological structures.

3. MD simulation results and discussion

3.1. Static properties

Figure 2 shows the local volume fraction of monomers for chains with the same monomer number of 62 but different ring numbers, which demonstrate the topological constraint of ring polymers. Here, the monomer volume fraction in the brush is the statistical average of the contributions of configurations ending up at different positions. It is also called monomer density in this paper.

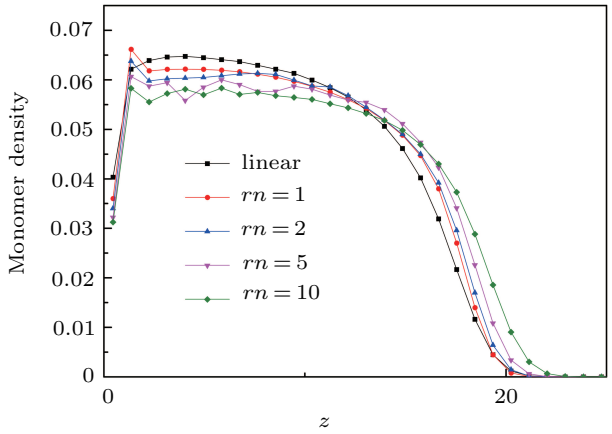


Fig. 2. (color online) Monomer density profiles along the z direction for ring polymer chains with different topological constraint values rn at grafting density $\rho = 0.1d^{-2}$ (62 monomers per chain).

As shown in Fig. 2, we see more monomers occupying the upper space of polymer brushes as ring number increases. In order to investigate how topological constraint impacts the size of ring polymer chains, we calculated the mean square radius of gyration $\langle R_G^2 \rangle$, which is defined as the average square distance between monomers

$$\langle R_G^2 \rangle = \frac{1}{N}\sum_{i=1}^{N}\langle (r_i - r_{cm})^2 \rangle = \frac{1}{N^2}\sum_{i=1}^{N}\sum_{j=1}^{N}\langle (r_i - r_j)^2 \rangle, \quad (6)$$

where r_i refers to the monomer position vector, and r_{cm} is the polymer's center of mass.

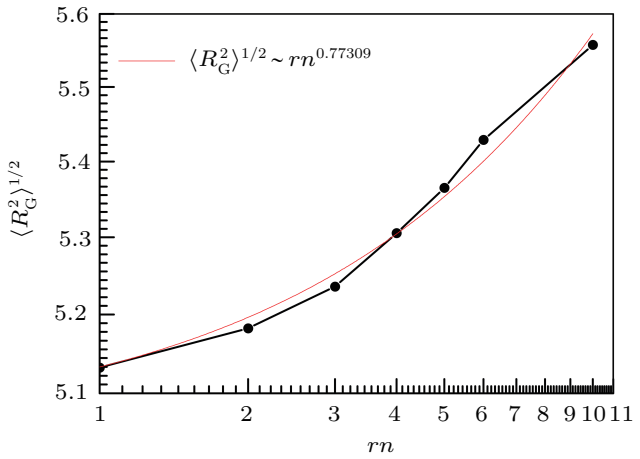


Fig. 3. (color online) The radius of gyration $\langle R_G^2 \rangle^{1/2}$ for polymer brush versus topological constraint values rn at grafting density $\rho = 0.1d^{-2}$ and chain length $N = 62$. The curve shows an exponential dependence with an exponent $\gamma = 0.77$.

From Fig. 3, we find a power law of radius of gyration with respect to topological constraint value $\langle R_G^2 \rangle^{1/2} \sim (rn)^{\gamma}$ with an exponent $\gamma = 0.77$. The SCF theory by Milner *et al.*[33] and Alexander[34] both predicted that the height of linear polymer brushes can be scaled as a power law in terms of molecular weight and grafting density: $h \sim N\rho^{1/3}$. The general physical picture depicted by Alexander[34] for the regime of high grafting density in a good solvent has shown that a grafted chain can be treated as linear arrays of blobs of size ξ ($\xi = \rho^{-1/2}$), which is the average distance between grafted sites on the surface. Each blob contains a number of $n_B = N/n = N\rho^{5/6}$ monomers. Thus, this gives the height scaled as $h \sim N\rho^{1/3}$, and the monomer concentration c scaled as $c \sim \rho^{2/3}$. To measure the height of a ring polymer chain, we also calculate the center-of -mass height H_{cm} by integrating over the monomer density profiles via

$$H_{cm} = \frac{\int_0^{\infty} z\phi(z)\,dz}{\int_0^{\infty} \phi(z)\,dz}. \quad (7)$$

We now take a look at the center-of-mass height $h \sim N^{\upsilon}$ for polymer chains with various topological constraints. As shown in Fig. 4, for the ring polymer with topological constraint $rn = 1$, one gets an exponent $\nu = 0.99$, a result with no significant difference from $\nu = 1.00$ for linear polymers and theory $\nu = 1$. However, as the topological constraint value gets larger, one sees a decreasing exponent, indicating that ring polymers with large topological constraint value get a weak power law. With the increase of topological constraint, the range of motion of the monomer becomes smaller, if compared with that of a linear polymer. Thus exponential relationship between the polymer chain size and the number of monomers is less significant with the increase of topological constraints (get a smaller exponential value).

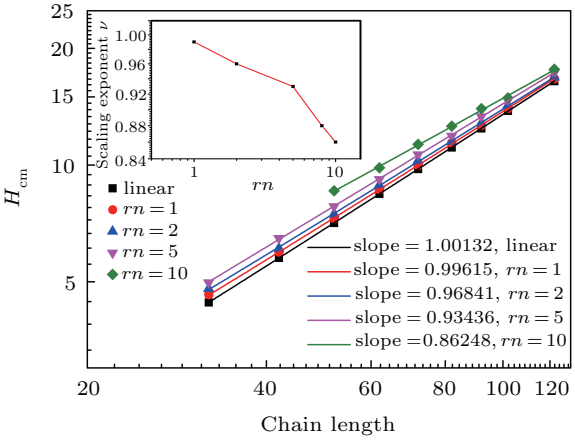


Fig. 4. (color online) The center-of-mass height H_{cm} for polymer brushes with different topological constraints versus chain length N at grafting density $\rho = 0.1d^{-2}$ and chain length $N = 62$. The inset shows the scaling exponent ν as a function of topological constrain value, indicating a less sensitive dependence of structure height on chain length.

In addition, the static properties of different topological structure on variant grafting density were studied, Figure 5 shows how the average radius of gyration $\langle R_{gz}^2 \rangle^{1/2}$ along the z direction depends on grafting density for polymer chain with different topological constraints. The linear chains exhibit scaling behavior $\langle R_{gz}^2 \rangle^{1/2} \sim \rho^{\nu}$ with scaling exponent $\nu = 1/3$ as expected. Ring polymer chains with topological constraint possess smaller scaling exponents, as shown in Fig. 5. For ring polymer brushes of a given chain length, one also sees two regimes, i.e., the low-density mushroom regime, where polymer chains hardly interact with each other, and the large-density brush regime, where chains are strongly overlapping. It is found that ring polymers with topological constraints, due to the good-solvent interaction, have lower probability collapsing than linear polymer, and thus correspond to a wider mushroom regime and a smaller scaling exponent.

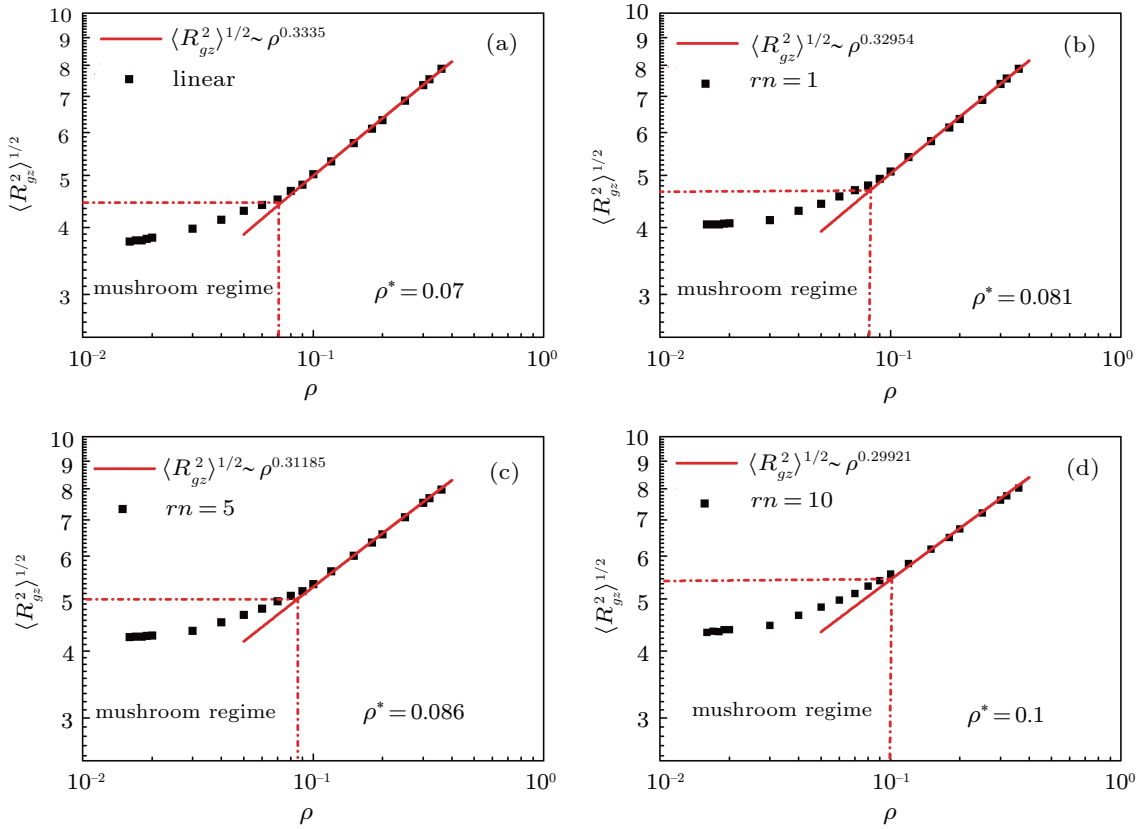


Fig. 5. (color online) The radius of gyration $\langle R_{gz}^2 \rangle^{1/2}$ for the z direction versus grafting density for chain length $N = 62$. ρ^* characterizes the critical density for the mushroom regime.(a) Linear polymer brushes, (b) ring polymer brushes with topological constraint value $rn = 1$, (c) ring polymer brushes with topological constraint value $rn = 5$, (d) ring polymer brushes with topological constraint value $rn = 10$. A larger mushroom region and smaller exponent are found as the topological constraint is enhanced.

3.2. Chain energy and bond force

In the polymer brush regime, as monomers tie together via a covalent bond, it is important to know the behaviors of bond force and energies, which can be calculated in the simulation. From the FENE bond energy defined by Eq. 3, a simple calculation yields

$$\boldsymbol{F} = \langle \nabla U_{\mathrm{FENE}}(\boldsymbol{r}) \rangle = \left\langle -\boldsymbol{r} \left(\frac{KR_0^2}{r^2 - R_0^2} + \frac{4\varepsilon}{r^2} \left[12 \left(\frac{d}{r} \right)^{12} - 6 \left(\frac{d}{r} \right)^{6} \right] \right) \right\rangle. \tag{8}$$

Figure 6 shows the z-component force for the polymer chains with different topological structures. In both the linear polymer chains and the ring polymer chains, the first bond connecting the grafted monomer and the first movable monomer, exhibits

particularly high stretching force. In the ring polymers, the z-component force distributes symmetrically and smoothly along the two branches except the one connecting the neighboring rings. As shown in Fig. 2, monomers close to the substrate seem to be much more compact than those on the top, due to the decreasing bond force with the monomer's position.

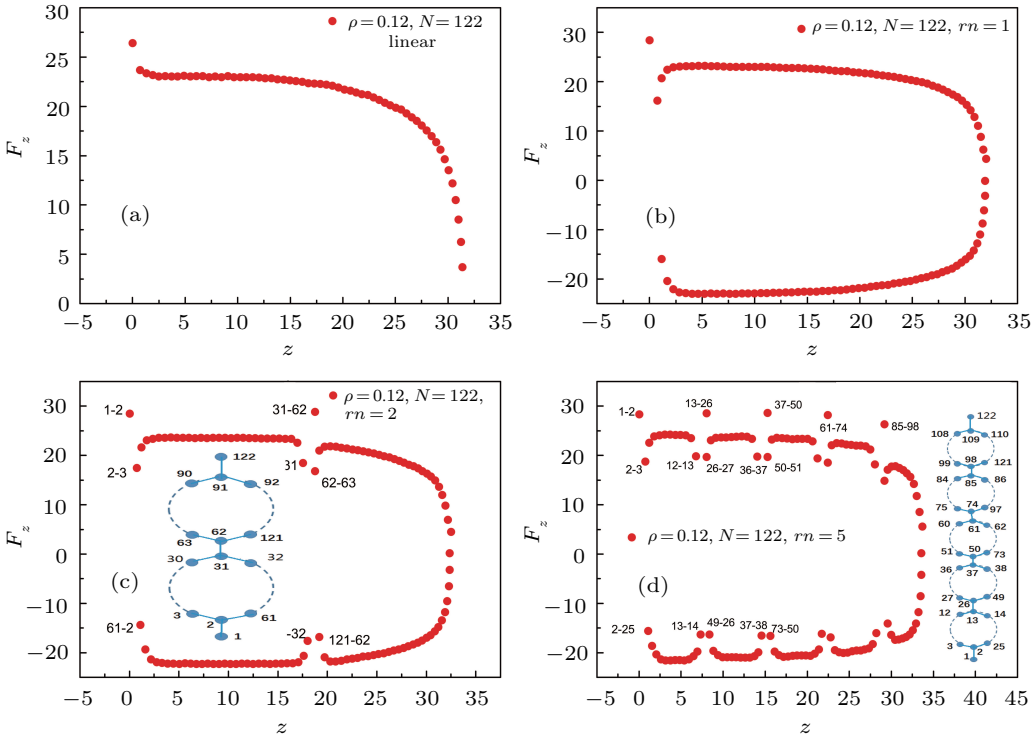


Fig. 6. (color online) Average bond forces along the z direction for ring polymers with chain length $N = 122$ for various topological constraint value rn as a function of the distance from the surface. (a) Linear polymer brushes, (b) ring polymer brushes with topological constraint value $rn = 1$, (c) ring polymer brushes with topological constraint value $rn = 5$, (d) ring polymer brushes with topological constraint value $rn = 10$.

The stretching energy of each chain is obtained by integrating the force along the z direction. As pictured by Alexander, each chain is a stretched array of tension blobs, with each blob corresponding to an order of thermal energy $k_{\rm B}T$. The total stretching energy of each chain is $k_{\rm B}T$ times its number of blobs:

$$F_{\rm ene} \sim \frac{N}{g} \sim N\rho^{1/2\upsilon} \sim N\rho^{5/6}. \tag{9}$$

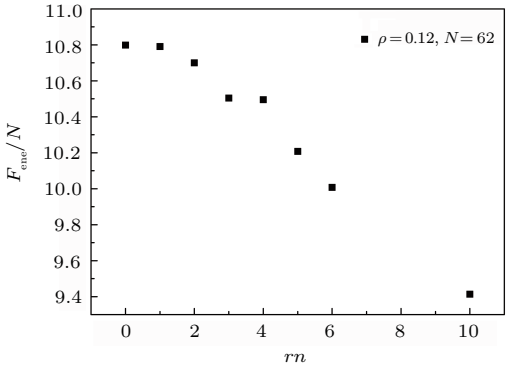


Fig. 7. Stretching energy scaled with number of bonds per chain as a function of topological constraint value.

As shown in Fig. 7, the stretching energy of each chain per number of bonds decreases with the topological constraint value. Figure 8 is a master curve exhibiting the stretching energy per number of bonds as a function of grafting density ρ for different topological structures. Linear polymer brush in moderate and high grafting density agrees perfectly well with the theoretical result Eq. 9. However, slightly larger exponents υ are found for ring polymer brushes, and the larger the topological constraint value, the larger the exponent.

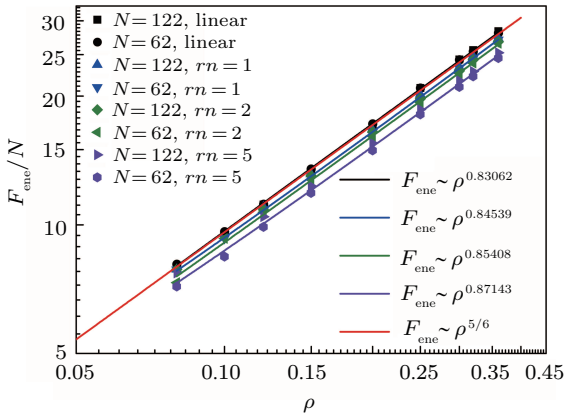


Fig. 8. (color online) Stretching energy scaled with number of bonds per chain as a function of grafting density for different topological structures.

3.3. End monomer

Figure 9 shows the distribution of end-monomers for linear chains and ring polymer chains with various topological structures, a different picture in contrast to the "Alexander brush".[34] It is found from Fig. 9 that under the same grafting density, as the topological constraint value increases, the end-

monomer distribution shifts to a higher position, indicating that the end monomers of ring polymer with topological constraint value tend to occupy the higher position of the brush. This conclusion is clearer from Fig. 10(a), illustrating that a ring polymer brush with larger topological constraint values is more compact at the upper region of the brush as a result of the effective excluded-volume effect. This can also be supported by the bond force connecting the end monomer, which becomes larger as the polymer chains own a more complex topological structure, as shown in Fig. 10(b).

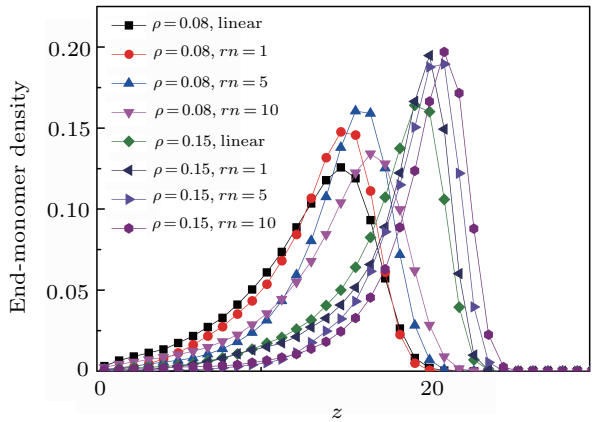


Fig. 9. (color online) The end-monomer density profiles with various topological constraint values for grafting density $\rho = 0.08$ and $\rho = 0.15$.

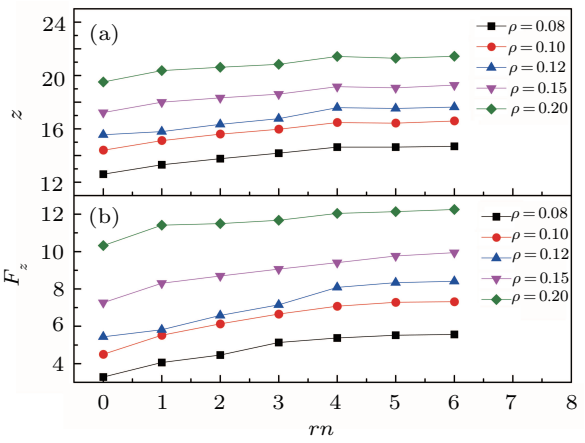


Fig. 10. (color online) (a) The end-monomer height as a function of the topological constraint value *rn* for various grafting densities. (b) The force of the bond connecting the end monomer as a function of the topological constraint value *rn* for various grafting densities.

3.4. Isothermal compression of the brush

In order to understand the different behaviors of brushes with different topological structure polymer under pressure, a movable wall made of athermal monomers is placed in the system to compress the brush. Between the wall and the remaining monomers of the brush exists only the repulsive short-range LJ-interaction. The compression is slow enough so that the brush stays in equilibrium during the whole process. Figure 11 displays the brush height for polymer brushes with different topological structures as a function of external compression force f_z. It is found that the brush height, insensitive to topological structure, decreases sharply and then levels off at the large compression force regime. This is because in the large force regime, the monomer structure inside the brush becomes close-packing and it becomes more difficult to compress the brush.

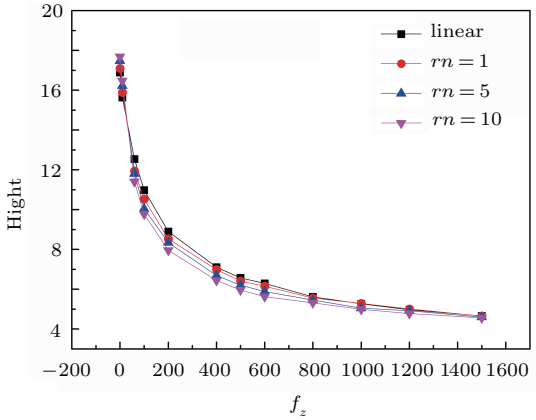


Fig. 11. (color online) Brush height as a function of external vertical force f_z for different topological structure polymer brushes.

In our simulation it is possible to obtain the average monomer concentration by integrating vertical monomer density profiles ϕ:

$$\langle c\rangle = \frac{\int_0^\infty \phi^2(z)\,\mathrm{d}z}{\int_0^\infty \phi(z)\,\mathrm{d}z}. \tag{10}$$

We can also calculate free energy by computing the minimal work $W_{\min} = \Delta F$ needed to accomplish the compression of the brush to a given height.

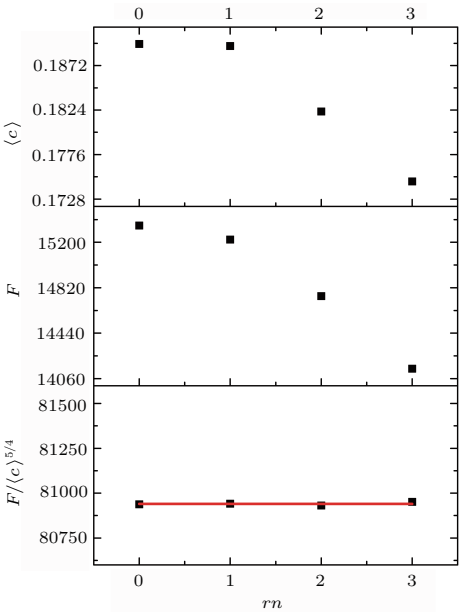


Fig. 12. (color online) Average monomer concentration versus topological constraint value *rn* (upper panel), free energy versus topological constraint value *rn* (central panel), and free energy scaled with $\langle c\rangle^{5/4}$ versus topological constraint value *rn* (lower panel).

From Fig. 2, it has been noted that topological constraint impacts the distribution of monomers in a brush. Here it is also

found that the average monomer concentration and the free energy all decreases with the topological constraint, as shown in Fig. 12. From the scaling law we have already known the relationships $\langle c\rangle \sim \rho^{2/3}$ and $F \sim \rho^{5/6}$,[33] and thus the relationship $F \sim \langle c\rangle^{5/4}$ can be obtained. Given this, the free energy, after being scaled by $\langle c\rangle^{5/4}$, is found to be a topological invariant, as shown in the lower panel of Fig. 12.

4. Summary

In summary, an MD simulation has been performed to study ring polymers in good solvent, with different topological constraints and short or moderate chain length. For the center-of-mass height of a ring polymer brush scaled by chain length $h \sim N^{\nu}$, there is no significant difference of exponent from that of a linear brush in the small topological constraint regime. However, as the topological constraint becomes stronger, one obtains a smaller exponent. There also exists a master scaling power law of the total stretching energy scaled by chain length N for moderate chain length regime, $F_{\rm ene} \sim N\rho^{\nu}$, for ring polymer brushes, but with a larger exponent ν than 5/6, indicating an influence of topological constraint to the dynamic properties of the system, such as stretching energy. Upon compressing ring polymer brushes, the free energy scaled by $\langle c\rangle^{5/4}$ is found to be a topological invariant.

References

[1] de Gennes P G 1980 *Macromolecules* **13** 1069
[2] Milner S T 1991 *Science* **251** 905
[3] Netz R R and Andelman D 2003 *Phys. Rep.* **380** 1
[4] Jun S and Mulder B 2006 *Proc. Natl. Acad. Sci. USA* **103** 12388
[5] des Cloizeaux J 1974 *Phys. Rev. A* **10** 1665
[6] van Rensburg E J J 2009 *J. Phys. A: Math. Theor.* **42** 323001
[7] Deguchi T and Tsurusaki K 1997 *Phys. Rev. E* **55** 6245
[8] Shimamura M K and Deguchi T 2002 *Phys. Rev. E* **65** 051802
[9] Cates M E and Deutsch J M 1986 *J. Phys.* (France) **47** 2121
[10] Rubinstein M 1986 *Phys. Rev. Lett.* **57** 3023
[11] Hur K, winkler R F and Yoon D Y 2006 *Macromolecules* **39** 3975
[12] Ida D, Nakatomi D and Yoshizaki T 2010 *Polym. J.* **42** 735
[13] Dobay A, Dubochet J, Millett K, sottas P E and Stasiak A 2003 *Proc. Natl. Acad. Sci. USA* **100** 5611
[14] Roovers J and Toporowski P M 1983 *Macromolecules* **16** 843
[15] McKenna G B, Hostetter B J, Hadjichristidis N, Fetters L J and Plazek D J 1989 *Macromolecules* **22** 1834
[16] Cho D, Park S, Kwon K and Chan T 2001 *Macromolecules* **34** 7570
[17] Takano A, Kushida Y, Ohta Y, Masuoka K and Matsushita Y 2009 *Polymer* **50** 1300
[18] Takano A, Ohta Y, Masuoka K, Matsubara K, Nakano T, Hieno A, Itakura M, Takahashi K, Kinugasa S, Kawaguchi D, Takahashi Y and Matsushita Y 2012 *Macromolecules* **45** 369
[19] Liu Y and Chakraborty B 2008 *Phys. Biol.* **5** 026004
[20] Forgan R S, Sauvage J P and Stoddart J F 2011 *Chem. Rev.* **111** 5434
[21] Pakula T and Geyler S 1988 *Macromolecules* **21** 1665
[22] Brown S and Szamel G 1998 *J. Chem. Phys.* **109** 6184
[23] Muller M, Wittmer J P and Cates M E 2000 *Phys. Rev. E* **61** 4078
[24] Muller M, Wittmer J P and Barrat J L 2000 *Europhys. Lett.* **52** 406
[25] Vettorel T, Grosberg A Y and Kremer K 2009 *Phys. Biol. Jpn.* **6** 025013
[26] Takano A 2007 *Polm. Prepr. Jpn.* **56** 2424
[27] He S Z, Merlitz H, Su C F and Wu C X 2013 *Chin. Phys. B* **22** 016101
[28] Sakaue T 2011 *Phys. Rev. Lett.* **106** 167802
[29] Suzuki J, Takano A and Matsushita Y 2013 *J. Chem. Phys.* **138** 024902
[30] Trefz B and Virnau P 2015 *J. Phys.: Condens. Matter* **27** 354110
[31] Flikkema E and Brinke G 2000 *J. Chem. Phys.* **113** 11393
[32] Plimpton S J 1995 *J. Comput. Phys.* **7** 1
[33] Milner S T, Witten T A and Cates M 1988 *Macromolecules* **21** 2610
[34] Alexander 1977 *J. Phys.* (France) **38** 977